BIOPHYSICS

FLIPs: Genetically encoded molecular biosensors for functional imaging of cell signaling by linear dichroism microscopy

Paul Miclea[1,2], Vendula Nagy-Marková[1,2], Robin Van den Eynde[3], Wim Vandenberg[3], Alina Sakhi[4], Alexey Bondar[1,5,6], Jitka Myšková[1], Peter Dedecker[3,7], Josef Lazar[1,2]*

Genetically encoded fluorescent biosensors convert specific biomolecular events into optically detectable signals. However, imaging biomolecular processes often requires modifying the proteins involved, and many molecular processes are still to be imaged. Here, we present a biosensor design that uses a hitherto overlooked detection principle: directionality of optical properties of fluorescent proteins. The biosensors (termed FLIPs) offer an extremely simple design, high sensitivity, multiplexing capability, ratiometric readout, and other advantages, without requiring modifications to their targets. We demonstrate the sensor performance by real-time imaging activity of G protein–coupled receptors (GPCRs), G proteins, arrestins, and other membrane-associated proteins, as well as by identifying a previously undescribed, pronounced, endocytosis-associated conformational change in a GPCR–β-arrestin complex. In combination with an original tri-scanning linear dichroism confocal microscope, FLIPs allow unparalleled imaging of activity of nonmodified, endogenously expressed G proteins. Thus, FLIPs establish a powerful molecular platform for imaging cell signaling, allowing numerous future developments and insights.

INTRODUCTION

Genetically encoded fluorescent biosensors allow visualizing specific cellular processes in living cells, tissues, and animals. Such probes are often constructed by fusing a sensing protein to a fluorescent moiety [such as a fluorescent protein (FP)], creating a causal connection between the molecular process of interest and the fluorescence output (*1*, *2*). Usually, a conformational or structural change in the sensing protein is used to modulate one of several modes of fluorescence quenching, most often through facilitating (or restricting) access of water molecules to the fluorophore (e.g., in circularly permuted FPs) or through providing (or removing) a suitable excitation energy donor or acceptor [e.g., in bioluminescence resonance energy transfer or fluorescence resonance energy transfer (FRET)]. The requirement for a sufficiently large conformational change in the sensing protein severely limits the number of phenomena that can be probed. Furthermore, many such molecular biosensors require an insertion of a fluorescent moiety into the protein of interest (e.g., a receptor protein), leading to potential perturbations in its function. Although so-called translocation sensors, responding by redistribution of a fluorophore across the cell (*3*, *4*), avoid the need for a conformationally switching protein, their responses are slow, and their number of targets is limited. Thus, there remains a strong need for biosensors that would allow real-time in vivo observations of the dynamic functional activity of a wide range of nonmodified, endogenously expressed proteins, providing quantifiable, ratiometric readout while allowing multiplexing.

To try to meet this need, we decided to exploit the well documented, but seldom used effects of optical directionality of FPs. Fluorescent molecules (including FPs) behave like dipole antennas, with pronounced directional properties (*5*, *6*). Molecular directional properties can cause differences in the rates of absorption of light of distinct linear polarizations [linear dichroism (LD)], as well as fluorescence polarization. The two phenomena can report on the molecular orientation (or orientational distribution) at the time of light absorption and emission by the fluorophore, yielding quantitative insights into the protein structure and its dynamics not accessible by other means. Although observations of these phenomena offer intrinsically ratiometric readout, allow multiplexing (due to the need for only a single spectral band), and are relatively simple to implement, they have so far found only niche applications in biological microscopy (*7*–*13*). This is because the existing biosensors based on molecular optical directionality have fundamental drawbacks: They modify the proteins of interest (*14*) and require a specific design for each application. Furthermore, their responses are usually small (*15*), and efforts at improvements have largely been nonproductive (*8*, *15*). For optical directionality to become a mainstream tool of biomolecular microscopy, these drawbacks would have to be overcome.

To address these challenges, we have conceived a class of molecular probes that we term fluorescence anisotropy and linear dichroism probes (FLIPs) (Fig. 1A). A FLIP includes four distinct functional components: a fluorescent moiety (i) (such as an FP), bearing at one of its termini a flexible linker (ii) and a membrane-targeting moiety (iii), and at the other terminus a moiety capable of binding the target of the probe (iv). We hypothesized that, in the absence of the probe's target, the FP moiety would adopt a largely random molecular orientation, while, in presence of the target, the orientation of the FP with respect to the cell membrane would become restricted. These changes in FP orientation could then be easily revealed by observing the optical directionality of the fluorescent moiety through observations of LD (Fig. 1B).

[1]First Faculty of Medicine, Charles University in Prague, Kateřinská 32, 121 08 Prague, Czechia. [2]Innovative Bioimaging, s.r.o., Podolská 1490/6, 147 00 Prague 4, Czechia. [3]Department of Biochemistry, Molecular and Structural Biology, KU Leuven, Celestijnenlaan 200G, 3001 Heverlee, Belgium. [4]Institute of Organic Chemistry and Biochemistry, Czech Academy of Sciences, Flemingovo nám. 2, 160 00 Prague, Czechia. [5]Institute of Plant Molecular Biology, Biology Center of the Czech Academy of Sciences, Branišovská 1160/30, Budweis, Czechia. [6]University of South Bohemia, Faculty of Science, Branišovská 1160/30, Budweis, Czechia. [7]Université de Lille, LASIRe CNRS, 59655 Villeneuve, France.
*Corresponding author. Email: josef.lazar@lf1.cuni.cz

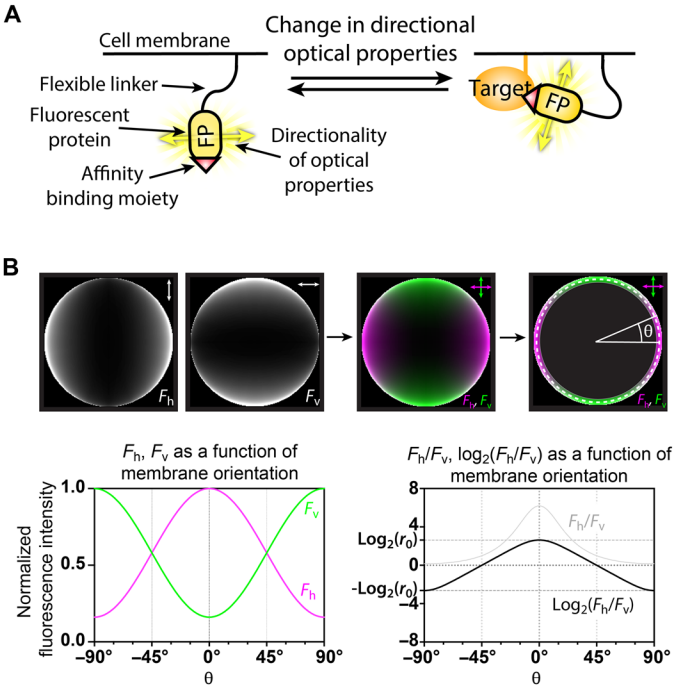

Fig. 1. General design of FLIPs and the detection principle. (**A**) A general structure of a fluorescence anisotropy and linear dichroism probe (FLIP), consisting of a membrane anchor, a flexible linker, a fluorescent moiety, and an affinity binding moiety. Upon binding of the affinity moiety to a target, the orientation of the fluorescent moiety changes. This is detectable by observations of LD. (**B**) Observing and quantitating LD, illustrated on a mathematical model of a simplified spherical cell. Imaging with two distinct linear polarizations of the excitation light generates two fluorescence images (F_h and F_v, obtained with light polarized horizontally and vertically in the image, respectively). LD is visualized by coloring the two images magenta and green and overlaying (optionally including a color contrast adjustment). For LD quantitation, the membrane area is segmented and the membrane orientation in each pixel is described by an angle θ. This yields sine- and cosine-like relationships of fluorescence intensities F_h and F_v on θ. To characterize the LD of a particular construct, the value of F_h/F_v for $\theta = 0$ (denoted as r_0) may be used. However, it is preferable to use $\log_2(r_0)$ [that is, $\log_2(F_h/F_v)$ at $\theta = 0$], as $\log_2(F_h/F_v)$ follows a robust, sine-like relationship on θ, permitting the value of $\log_2(r_0)$ to be accurately inter- or extrapolated from $\log_2(F_h/F_v)$ values for $\theta \neq 0$ (*19*). In our previous works, $\log_2(r_0)$ was denoted as $\log_2(r_{max})$.

The exceedingly simple and versatile molecular design promises to address all of the abovementioned drawbacks of existing biosensors based on optical directionality. The target molecules do not need to be modified in any way. By virtue of its clear molecular mechanism of function, simplicity, modularity, and versatility, the FLIP molecular architecture provides a single design readily applicable to rapid development of biosensors for many distinct molecular targets. The expected robust, predictable changes in molecular orientation of the fluorescent moiety should yield strong observable signatures, tunable by targeted modifications to the distinct parts of the sensor molecules. FLIPs should benefit from the inherent advantages of optical directionality measurements, namely, a ratiometric readout resistant to bleaching artifacts, and the need for only a single spectral channel, allowing to combine FLIPs with other fluorescent constructs, including other biosensors. Driven by the high promise of the FLIP biosensor design, we set out to investigate its applications to a range of intracellular molecular processes.

RESULTS

Initial FLIP designs

For our initial attempts, we chose to develop a FLIP that would report on the presence of the activated form of the G protein Gαi1. Gαi1 plays an important role in physiology, by transducing signals from numerous G protein–coupled receptors (GPCRs) (*4*). Moreover, Gαi1 signaling had been investigated both by polarization microscopy (using constructs with an FP inserted into the Gα subunit) (*8*, *14*, *15*) and other methods, such as FRET or bimolecular fluorescence complementation between G protein subunits (*2*, *16*), allowing comparison with the current approach. We chose the peptide KB1753, known to bind activated Gαi subunits (*16*, *17*), as the affinity binding moiety. The enhanced green fluorescent protein (eGFP) served as the fluorescent moiety, and the hexapeptide Gly-Ser-Gly-Gly-Ser-Gly as the flexible linker. As membrane anchors (*18*), we tested the N-terminal palmitoylation signal peptide derived from GAP43, the transmembrane domain of the interleukin receptor IL4Rα, the C-terminal palmitoylation/farnesylation domain of H-Ras, and the C-terminal farnesylation domain of K-Ras.

To determine whether the four probes (GAP43-eGFP-KB1753, IL4R-eGFP-KB1753, KB1753-eGFP-HRas, and KB1753-eGFP-KRas) interact with the intended target, we observed their LD (differences in fluorescence intensities upon excitation with distinct linear polarizations of light) in living human embryonic kidney (HEK) 293 cells, in the absence and presence of a constitutively active mutant of Gαi1 (denoted as Gαi1*). The extent of LD was quantitated as the dichroic logratio [$\log_2(r_0)$], that is, by the logratio of fluorescence intensities elicited by light polarized horizontally and vertically [$\log_2(F_h/F_v)$] in the image, in a section of the membrane with its normal oriented horizontally within the image (Fig. 1B) (*8*, *19*, *20*). Such ideal membrane orientation need not be present in the examined images, as the value of $\log_2(r_0)$ can be robustly extrapolated from almost any section of a membrane with a known orientation (*19*). Positive values of $\log_2(r_0)$ indicate an orientation of the fluorophore's transition dipole moment (TDM; a "molecular antenna") close to perpendicular to the membrane, while negative values imply a TDM orientation close to parallel to the membrane. Wide distributions of molecular orientations or orientations centered around the so-called "magic angle" (54.7°) yield values of $\log_2(r_0)$ close to 0. The results of our LD determinations are illustrated in Fig. 2 and figs. S1 and S2 and summarized in table S1. We observed notable differences in LD between cells expressing only a probe and those coexpressing the probe and Gαi1* for all constructs except GAP43-eGFP-KB1753. The effect was most pronounced in IL4Rα-eGFP-KB1753 which, however, showed irregular membrane localization (fig. S1). Thus, we selected KB1753-eGFP-HRas for further development and testing.

Modifying the length of the flexible linker brought little benefit (fig. S2). Extending the linker reduced the effect of Gαi1 presence on LD, presumably by increasing the orientational freedom of the eGFP moiety while engaged with Gαi1*. Probes with shorter linkers showed relatively high LD when expressed alone, and their LD was affected only little by presence of Gαi1*. This is consistent with the cell membrane proximity restricting the rotational freedom of the eGFP moiety and reducing the ability of the construct to bind Gαi1*. Thus, we used the original hexapeptide linker in our further studies.

Replacing the eGFP moiety with other FPs (Fig. 2, C and D) resulted in functional sensors that generated a strong LD contrast over a range of emission colors. However, the signs and magnitudes of

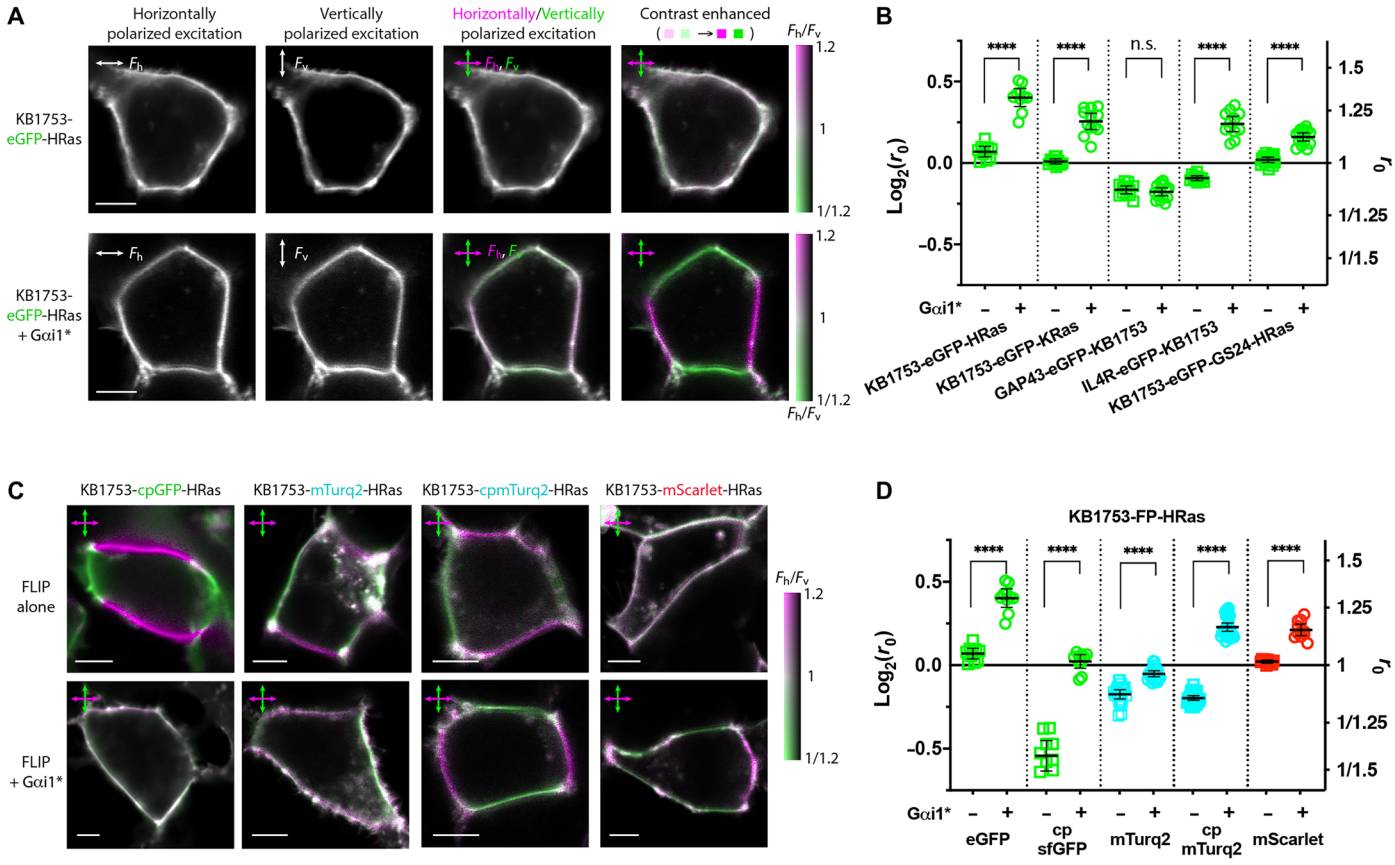

Fig. 2. Detecting the presence of a constitutively active mutant of Gαi1 (Gαi1*) by FLIPs and LD microscopy. (**A**) A HEK293 cell expressing KB1753-eGFP-HRas (top) and coexpressing KB1753-eGFP-HRas and Gαi1* (bottom). From left to right: Image acquired using excitation light polarized horizontally; image acquired using excitation light polarized vertically; the two preceding images colored magenta and green, respectively, and overlaid; same as in the preceding image, but the coloring adjusted to cover the shown range of dichroic ratios (F_h/F_v), as indicated by the color bar. In cells expressing Gαi1*, the FLIP exhibits pronounced LD. Scale bars, 5 μm. (**B**) LD of eGFP-bearing FLIPs containing various membrane anchors and linkers, in the absence and presence of Gαi1*. Means and 95% confidence intervals are indicated. With the exception of GAP43-eGFP-KB1753, all tested FLIPs exhibit significantly different LD in presence of Gαi1*. (**C**) Representative LD microscopy images of HEK293 cells expressing FLIPs of the KB1753-FP-HRas design, bearing various FPs. Coloring as in (A). Scale bars, 5 μm. Top: Cells expressing the indicated FLIP. Bottom: Cells coexpressing the indicated FLIP and Gαi1*. Differences in LD between cells expressing only a FLIP and coexpressing the FLIP and Gαi1* are apparent. Notably, cells expressing KB1753-cpmTurq2-HRas exhibit LD of a different sign in the absence and presence of Gαi1* (inversion of the magenta-green pattern). (**D**) LD of FLIPs of the KB1753-FP-HRas design, bearing different FP moieties. Means and 95% confidence intervals are indicated. Presence of Gαi1* had a significant effect on the LD of all tested FLIPs. Marked differences between the distinct FLIPs are apparent. ****$P < 0.0001$; n.s., not significant.

the contrast could differ between the FPs in unexpected ways. As expected, modifying the orientation of the fluorophore with respect to the cell membrane by circular permutation of the FP moiety [cpsfGFP (*21*) and cpmTurq2 (*22*)] affected the LD of the respective sensors, both in the absence and presence of Gαi1*. Unexpectedly, some FLIPs (namely, KB1753-cpsfGFP-HRas and KB1753-mTurq2-HRas) showed higher LD in the absence of Gαi1* than in its presence. Some highly similar constructs (KB1753-eGFP-HRas and KB1753-mTurq2-HRas) exhibited opposite Gαi1*-induced behaviors. A particularly notable kind of contrast was observed in KB1753-cpmTurq2-HRas, which showed opposite signs of LD in the absence and in the presence of Gαi1*, allowing simple, unambiguous visual identification of different conformational states of the FLIP even without LD quantitation. The results obtained in attached cells are consistent with our single- and two-photon LD microscopy observations of cells made spherical by hypotonic treatment (fig. S3), which allow determinations of TDM orientations with respect to the membrane (table S2) (*19*). This information currently does not allow determinations of orientations of the FP β barrel. However, our knowledge of TDM orientations within the FP molecules (*6*) implies divergent FP orientations even between nearly identical FLIP (particularly between the eGFP/mTurq2 versions; less so in cpsfGFP/cpmTurq2). We attribute the observed idiosyncratic behaviors of these constructs to sequence-specific interactions between the FP moiety and the plasma membrane. In the future, such interactions may be exploited in rational development of improved FLIPs. Overall, our results demonstrate that FLIPs can deliver useful biosensors using a wide range of FPs spanning a broad region of the visible spectrum.

Observing activation of Gαi1

We then explored whether the Gαi1* probes could also report on the activation and inactivation of nonmodified Gαi1 (Fig. 3). To ensure close to equimolar concentrations, we observed cells overexpressing

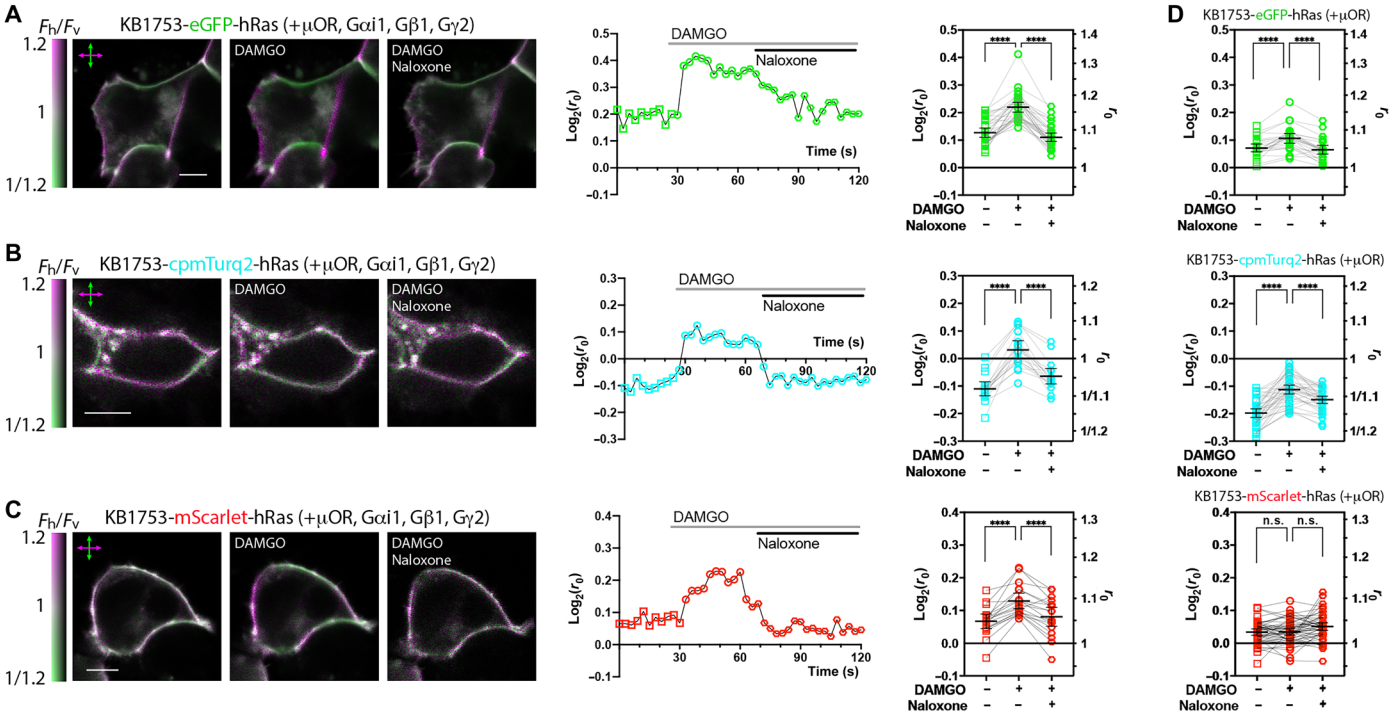

Fig. 3. Imaging activity of Gαi1 by LD microscopy and FLIPs of the KB1753-FP-HRas design. (**A** to **C**) HEK293 cells overexpressing the μ-opioid receptor (μOR), Gαi1, Gβ1, Gγ2, and the indicated FLIP, imaged before and after addition of a μOR agonist (DAMGO) and after addition of an excess μOR antagonist (naloxone). (A) KB1753-eGFP-HRas; (B) KB1753-cpmTurq2-HRas; (C) KB1753-mScarlet-HRas. Left: LD microscopy images showing a cell before addition of DAMGO, after addition of DAMGO, and after addition of naloxone. All scale bars, 5 μm. Middle: Temporal profile of LD in response to μOR activation and inactivation of the shown cell. Right: LD of cells before activation, 30 s after addition of DAMGO, and 30 s after addition of naloxone. Changes in LD in response to addition of DAMGO and naloxone are apparent for all three FLIPs. (**D**) LD of HEK293 cells overexpressing μOR and the indicated KB1753-FP-HRas (not overexpressing any G protein), before and after addition of DAMGO and after addition of naloxone. Mean values and 95% confidence intervals indicated. ****$P < 0.0001$; n.s., not significant.

a KB1753-based FLIP, as well as nonmodified G proteins Gαi1, Gβ1, Gγ2, and the μ-opioid receptor (μOR). Before activation of the receptor, all three tested FLIPs (KB1753-eGFP-HRas, KB1753-cpmTurq2-HRas, and KB1753-mScarlet-HRas) exhibited LD somewhat higher than that of the probes overexpressed alone (Fig. 3). This is likely due to basal activity of μOR and other G_i-coupled GPCRs present in the cells, as well as to nonspecific binding of KB1753 to the nonactivated form of Gαi1. Upon addition of [D-Ala^2, N-MePhe^4, Gly-ol]-enkephalin (DAMGO), a full μOR agonist (*23*), the LD of all three probes quickly changed, in a direction consistent with our observations of the effects of Gαi1*. Cells expressing KB1753-cpmTurq2-HRas often changed the sign of LD (LD inversion, or LD "flip"), allowing easy visual identification of different functional states of Gαi1.

The responses of all three FLIPs were smaller than those observed in our experiments with Gαi1*, likely due to incomplete activation of the Gαi1 pool by μOR. Upon addition of an excess of a μOR antagonist (naloxone) (*16*), the LD of all three FLIPs returned to values close to those observed before μOR activation, with residual responses likely due to continuous presence of DAMGO. The kinetics of the observed responses to μOR activation/inactivation were in agreement with previous observations (*8*), suggesting that the binding of the FLIP to the activated Gαi1 does not substantially affect the G protein activation or inactivation. Our results show that FLIPs can be used for real-time single-cell imaging, with subcellular resolution, of the activation and inactivation of nonmodified, overexpressed G proteins, exceeding the abilities of other sensors (*2*) by providing similar or better signal-to-noise, while not requiring that the targets be modified.

The ability of FLIPs to image activity of nonmodified G proteins led us to investigate whether FLIPs can report on the activity of endogenously expressed G proteins. We tested this possibility by observing cells overexpressing a Gαi-detecting FLIP and the μOR (allowing reliable Gαi activation) but expressing G proteins endogenously (Fig. 3D). Our results show that the LD of KB1753-eGFP-HRas and KB1753-cpmTurq2-HRas changes significantly both upon μOR activation by DAMGO and inactivation by naloxone. Unlike the other two FLIPs, KB1753-mScarlet-HRas showed no statistically significant changes in LD upon activation/inactivation of endogenously expressed Gαi, even after observing more than 50 cells. A possible explanation for this result is that the mScarlet moiety, having a distinct sequence and structure from the other two FPs, presents a steric hindrance that lowers the affinity of the KB1753 peptide toward its target.

The LD changes observed in cells overexpressing μOR and KB1753-eGFP-HRas or KB1753-cpmTurq2-HRas were in line with those we observed in cells that also overexpressed Gαi1, Gβ1 and Gγ2, but markedly smaller. On the basis of our measurements of LD in cells expressing Gαi1*, we estimated that about 15% of the FLIP molecules become bound to the endogenous Gαi upon activation. In theory, reducing the molar excess of the FLIP over the endogenous G_i might lead to a larger fraction of the FLIP becoming bound upon G_i activation and, in turn, to a larger and more easily discernible

change in LD. However, because we did not notice any relationship between the magnitude of the LD change and the FLIP expression level, we believe that the potential benefit of a lower FLIP concentration is being negated by the relatively low affinity of KB1753 for the activated Gαi subunits [dissociation constant (K_d) = ~1 μM] (*17*). Improving the sensitivity of detection of endogenous G protein signaling will likely require increasing the affinity of the FLIP binding moiety. Despite the limits imposed by the affinity of KB1753, our ability to image activation of nonmodified, endogenously expressed G proteins represents, to our knowledge, a first (*2*) and is likely to improve further with future developments.

Observing activation of GPCRs

Encouraged by our success in observing the activity of Gαi1, we expanded the range of FLIP probes to observe the activity of distinct GPCRs. The versatility of the FLIP design allowed us to create biosensors based on nanobodies NB33 and NB80, which specifically bind the activated forms of the μOR and the β2-adrenergic receptor (β2AR), respectively (Fig. 4) (*3*, *24*). Briefly, the LD of NB33-eGFP-HRas exhibited rapid LD inversion upon addition of DAMGO. The response could be reversed by application of naloxone. NB80-eGFP-HRas responded to the activation of β2AR (by isoproterenol) by rapid, robust LD inversion. The fluorescence intensity in a membrane whose normal is oriented horizontal in the image dropped by close to 50% with excitation polarized horizontally (F_h), while rising by 50% with excitation polarized vertically (F_v) (fig. S4A). In some cases, the LD inversion occurred during an image acquisition, demonstrating short response onset times of ~100 ms (fig. S4B), likely limited by agonist diffusion rates rather than by the biosensor kinetics. In contrast, the observed rate of β2AR inactivation by a β2AR inverse agonist (propranolol) was on the order of minutes. We reasoned that the high binding affinity of NB80 for β2AR [reported to be 3 nM for the isoproterenol-activated receptor; (*3*)] hindered the receptor leaving the active conformation. Thus, guided by the known structure of the β2AR-NB80 complex (Protein Data Bank ID 3P0G) (*25*), we mutated four amino acids of NB80 that form contacts with the active form of β2AR but away from the loop that fits into the central cavity of the activated receptor (fig. S5). The resulting FLIP (NB80Lite-eGFP-HRas) exhibits optical properties similar to NB80-eGFP-HRas, including a large, rapid response to β2AR activation, but exhibits virtually no affinity for the nonactivated receptor and a much faster response to β2AR inactivation than NB80-eGFP-HRas.

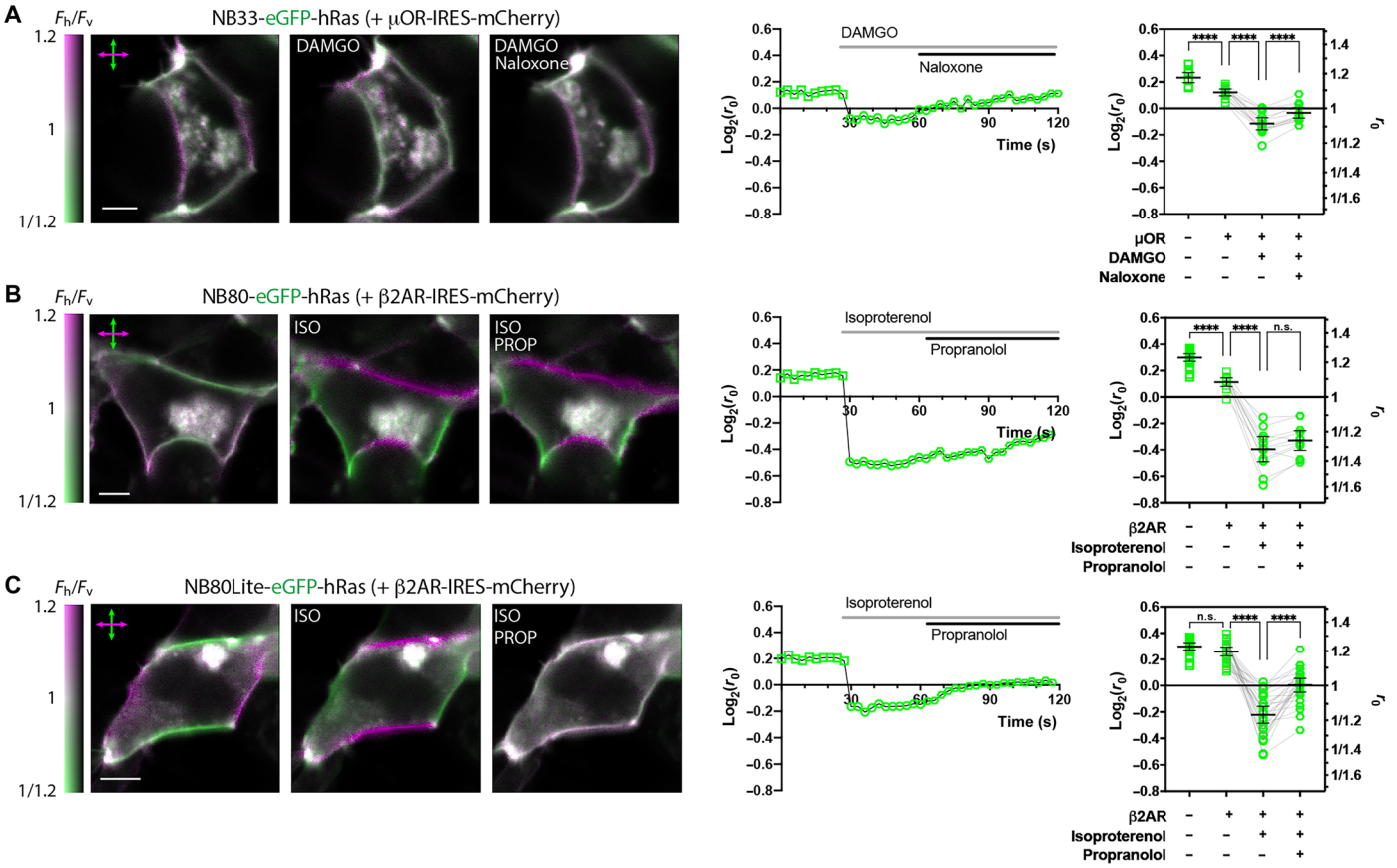

Fig. 4. Imaging GPCR activity by LD microscopy and FLIPs. (**A**) Imaging μOR activity in HEK293 cells overexpressing μOR-IRES-mCherry and NB32-eGFP-HRas. Left: A cell observed before stimulation, after μOR activation (by addition of DAMGO), and after μOR inactivation (by addition of naloxone). Middle: Temporal profile of LD during μOR activation and inactivation of the shown cell. Right: Values of LD observed in the absence of μOR and in its presence before stimulation, 30 s after activation, and 30 s after inactivation (each data point represents a single cell; mean values and 95% confidence intervals indicated). (**B**) β2AR activity in HEK293 cells overexpressing β2AR-IRES-mCherry and NB80-eGFP-HRas; isoproterenol (ISO) and propranolol (PROP) were used for β2AR activation and inactivation, respectively. (**C**) Imaging β2AR activity using NB80Lite-eGFP-HRas. All scale bars, 5 μm. ****$P < 0.0001$; n.s., not significant.

Our results demonstrate that FLIPs can be used for sensitive, real-time observations of the activity of nonmodified GPCRs. They also show that nanobodies can serve as affinity moieties in FLIPs while highlighting the importance of a suitable binding affinity of the FLIP for its target. In combination with our observations of KB1753-based probes, our results with NB80-based FLIPs place limits on the range of binding affinities suitable for FLIP applications (likely 10 to 100 nM, depending on the target concentration).

Endocytosis-associated rearrangement of GPCR-arrestin complexes

We next aimed to visualize arrestin-mediated signaling. Arrestins play an important role in GPCR signal transduction, complementing or competing with signaling by G proteins (*26*, *27*). The roles of G proteins and arrestins are compartmentalized, both spatially (cell membrane versus endosomes) and temporally (so-called first versus second wave of GPCR signaling) (*28*). Upon GPCR activation, arrestins can bind to the receptor's phosphorylated C terminus (partial engagement) or to both the C terminus and the GPCR's central cavity (full engagement) (*29*, *30*). Partial arrestin engagement might allow formation of GPCR–G protein–arrestin supercomplexes, whose existence has, however, only been demonstrated with purified, reconstituted proteins, under highly favorable conditions (*31*). In contrast, our approach promised real-time observations of arrestin molecular interactions in living cells, with subcellular resolution.

To detect interactions of arrestins with GPCRs, we prepared NB32-eGFP-HRas (*32*). This FLIP uses NB32, a nanobody specific for activated arrestins bound to the phosphorylated C terminus of a GPCR (*29*, *32*). To stimulate arrestin recruitment to a GPCR, we used the bradykinin receptor 2 (B2R) (*4*, *33*, *34*). Cells overexpressing nonmodified B2R, β-arrestin 1 (βArr1), and NB32-eGFP-HRas responded to activation by bradykinin by an increase in LD of the probe in the cell membrane (Fig. 5), likely corresponding to the formation of the fully engaged B2R-βArr1 complex. Membrane vesicles (endosomes), which formed upon internalization of the activated B2R, exhibited LD similar to that observed in the cell membrane of the activated cells. Thus, NB32-eGFP-HRas can detect activation of βArr1 both in the cell membrane and in endosomes.

To test whether NB32-meGFP-hRas can distinguish between different modes of arrestin binding to activated GPCRs, we prepared a βArr1 mutant [βArr1(FLD)], bearing a deletion of the finger-loop region. Such deletions have been shown (*29*) to augment arrestin's partial engagement with GPCRs, reducing the formation of fully engaged GPCR-arrestin complexes. In presence of βArr1(FLD), activation of B2R leads to an increase in LD of NB32-eGFP-HRas present in the cell membrane similar to that observed in presence of nonmutated βArr1. However, notably, upon internalization into endosomes, the LD of the probe undergoes an inversion. This is in contrast to the behavior observed with nonmutated βArr1 and likely corresponds to formation of partially engaged complexes of B2R with βArr1(FLD).

The endocytosis-associated LD inversion observed with βArr1-(FLD) is robust and highly reproducible and seems to occur irrespective of cellular localization (periplasmic/intracellular; Fig. 5A), expression levels (weakly/brightly fluorescent; Fig. 5A), or vesicle age (nascent/mature). Furthermore, vesicle size (investigated across vesicle diameters, 0.5 to 2 μm) has only a minor effect on the observed LD for both the wild-type and mutated βArr1 (fig. S6). The slightly smaller LD seen in smaller vesicles is likely due to higher inclusion of nonequatorial parts of the vesicles in the acquired images. Possible causes for the observed conformational change observed in βArr1(FLD) include B2R's interactions with the caveolin-associated (*35*, *36*) or clathrin-associated (*37*, *38*) endocytosis machinery, effects of the endosomal lipid composition (*39*), pH, membrane curvature (*40*), or a yet-to-be-identified process occurring during the formation of endosomes. Although all of these mechanisms are expected to act both on B2R-βArr1 and B2R-βArr1(FLD), we could only observe rearrangement in the latter. This likely reflects a difference between the affinities of B2R and βArr1 versus B2R and βArr1(FLD). Because distinct GPCRs are known to exhibit distinct affinities toward arrestins (*4*), our observations suggest that complexes between certain GPCRs and βArr1 (those that are of suitable affinities) might

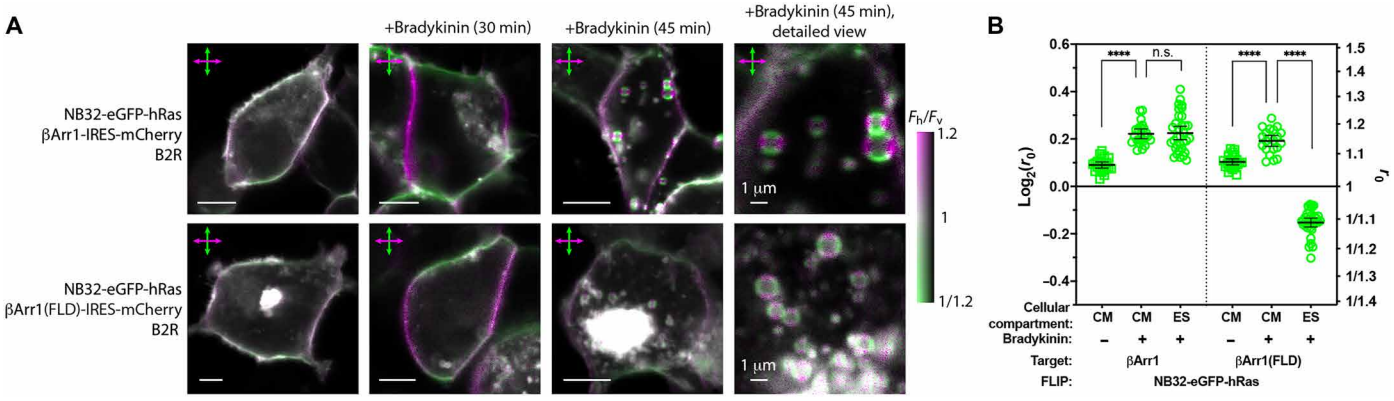

Fig. 5. Imaging arrestin signaling by LD microscopy and FLIPs. (**A**) Observations of NB32-eGFP-hRas in response to arrestin activation/recruitment due to stimulation of the bradykinin receptor (B2R) by bradykinin. Images of typical cells overexpressing B2R, NB32-eGFP-hRas, and βArr1 (top row) or βArr1(FLD) (bottom row) are shown. From left to right: Before application of bradykinin; 30 min after application of bradykinin; 45 min after application of bradykinin; and a detailed view showing endosomes, 45 min after application of bradykinin. Scale bars, 5 μm unless indicated otherwise. Cells overexpressing βArr1 and βArr1(FLD) exhibit similar LD responses in the cell membrane (CM) but markedly different responses in endosomes (ES) that emerge upon prolonged activation. (**B**) Quantitative analysis of LD of NB32-eGFP-hRas before and after activation of B2R in presence of βArr1 or βArr1(FLD) (mean values and 95% confidence intervals are indicated). ****$P < 0.0001$; n.s., not significant.

undergo rearrangement upon internalization, opening a possibility of downstream signaling bifurcation between distinct GPCRs. Intriguingly, the endosomal localization of the observed conformational transition is consistent with proposed mechanisms (*31*) that involve full engagement of arrestins with GPCRs in the cell membrane, followed by partial disengagement upon internalization (possibly accompanied by formation of supercomplexes GPCR–G protein–arrestin), leading to a so-called second wave of GPCR signaling.

Our observations of a previously unseen endocytosis-associated rearrangement of a GPCR-arrestin complex demonstrate the importance of the capacity of FLIPs and LD microscopy to visualize interactions between nonmodified GPCRs and arrestins with subcellular resolution. They also illustrate a unique ability to distinguish between distinct forms of protein-protein interactions. This ability, combined with the fact that the FLIP targets bear no modifications, opens doors to revealing hidden aspects of cell signaling, under conditions markedly closer to natural than previously possible.

Generalization of the FLIP concept

To explore the versatility of the FLIP design and a range of applications, we developed FLIPs containing the RH domain of GRK2 [known to bind the activated form of Gαq; (*41*)], nanobody NB35 [known to bind the activated form of Gαs; (*25*)]; the C-terminal domain of GRK2 [known to bind the Gβγ dimer often released upon activation of G protein heterotrimers; (*41*)], PAK1 [known to bind the activated form of the small GTPase RacA; (*42*)]; as well as a recently developed GP2-derived small affinity protein known (*43*) to bind to the ectodomain of the insulin receptor 1 (IR1) (fig. S7). The presence of their respective targets generally increased LD (that is, it increased the absolute values of the observed dichroic logratios), consistent with lowering the orientational freedom of the fluorescent moiety.

These observations illustrate the potential range of FLIP applications, which include studies of various G proteins (Gαq, Gαs, and Gβγ), function of small GTPases (activation of RacA, critical for embryonic development), or activity of receptor tyrosine kinases (i.e., the insulin receptor IR1, of crucial importance in diabetes). The results also show the range of molecules that can serve as binding moieties in FLIPs: peptides, nanobodies, and nanobody-like affinity scaffolds (such as GP2), as well as the natural binding partners (e.g., GRK2 and PAK1) of the target proteins. Conveniently, natural binding partners of endogenously expressed targets, by definition, are likely to exhibit affinities suitable for observations of targets expressed endogenously. Thus, our results open an avenue to observations of an exceedingly wide range of nonmodified, endogenously expressed signaling molecules, as long as the imaging setup provides sufficient sensitivity of fluorescence detection.

Fast and sensitive imaging of cell signaling dynamics using FLIPs and tri-scanning confocal LD microscopy

To investigate the speed and sensitivity limits of FLIP biosensors, we implemented LD microscopy on a simplified version of a recently developed (*44*) line-scanning confocal microscope (Fig. 6). In line-scanning confocal microscopy, the illuminating laser beam is focused into a line (rather than a spot), allowing acquisition of an entire confocal image by a camera within one sweep of the laser line. Using a single resonant scanning mirror for three separate functions ["tri-scanning" (*44*): scanning the laser beam across the sample, descanning the emitted fluorescence before its passage through a confocal slit, and scanning the fluorescence across the camera detector chip] eliminates synchronization issues and, therefore, maximizes the usable scanning speed. By simultaneous acquisition of a whole image column (1000 pixels) at a time, line scanning, in principle, delivers an up to a 1000-fold increase in image acquisition speed or sensitivity (*44*). In our hands, tri-scanning provides major improvements in imaging speed (routinely 10- to 20-fold) over standard point-scanning confocal microscopy, while delivering high detection sensitivity, low photobleaching (as lower per-pixel illumination intensities lead to lower deleterious light absorption by fluorophore triplet states), and an unexpectedly little reduction in image quality and resolution (movie S1).

We took advantage of the high image acquisition rate of the tri-scanning LD microscope, as well as of its low photobleaching, to observe the dynamics of the newly developed FLIP biosensors and to compare them to corresponding biosensors that respond by translocation (Fig. 6 and movies S2 and S3) (*3*, *24*). Briefly, all four investigated FLIPs responded virtually instantaneously, within a hundred milliseconds of addition of a suitable GPCR agonist. In contrast, the responses of translocation-based sensors were much slower, reaching their maximum approximately within 15 s. Translocating sensors that relied on NB80 and NB80Lite also developed pronounced LD while undergoing prominent translocation to the cell membrane (fig. S8 and movie S4). In contrast, translocation sensors using KB1753 and NB33 showed no detectable LD upon activation, consistent with the limited extent of their translocation.

Our results indicate that translocating sensors do not properly reflect the dynamics of GPCR activation. Rather, their response rates are limited by cytoplasmic diffusion across micrometer distances. In contrast, FLIPs, by virtue of their membrane localization, only need to diffuse across tens of nanometers, in two dimensions (*45*). Because diffusion times are inversely proportional to the square (in two-dimensional settings) or even to the cube (in three dimensions) of distance, FLIP responses are rapid, and much more accurately reflect the dynamics of GPCR activation. Our observations suggest that LD microscopy might yield information allowing to distinguish between molecular conformations of targets of translocation sensors that is not available from simple observations of the biosensors' cellular localization.

Last, we used the combination of speed and sensitivity provided by the tri-scanning microscope to explore the limits of detection sensitivity of the FLIP biosensors. We set out to confirm our finding (Fig. 3D) that FLIPs could report on the activity of the Gαi expressed endogenously in HEK293 cells. For these observations, we chose KB1753-eGFP-HRas, thanks to its robust responses to activation of overexpressed Gαi1 and longer excitation wavelength than KB1753-mTurq2-HRas. Markedly exceeding our results achieved with point-scanning LD microscopy, tri-scanning allowed us to detect LD changes consistent both with Gαi1 activation and inactivation by an overexpressed μOR, in real time, with subcellular resolution (Fig. 6C and movie S5). No changes in LD could be detected in the absence of the μOR or in cells expressing a construct consisting of a membrane-tethered GFP instead of the FLIP (fig. S9). The changes in LD observed by tri-scanning LD microscopy are consistent with those measured previously using point-scanning LD microscopy (Fig. 3D). The kinetics of activation of endogenous Gαi appear similar to those of the overexpressed Gαi1 (Fig. 3A), but with a slower on-rate (Fig. 6B), consistent with published evidence against GPCR–G protein preassembly (*15*). Thus, we conclude that the combination of FLIP biosensors and tri-scanning microscopy achieves the long-sought

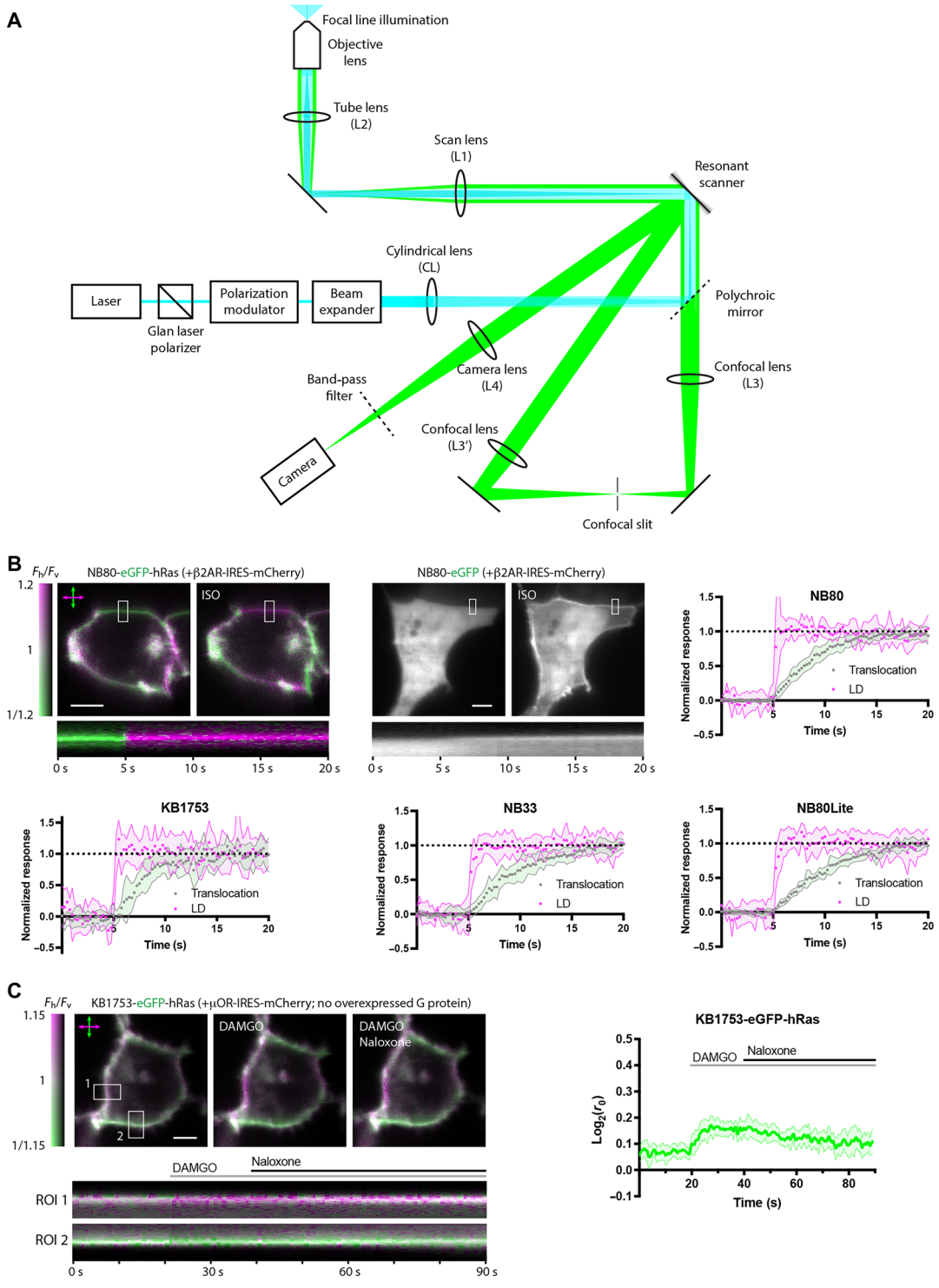

Fig. 6. Imaging of cell signaling by FLIPs and tri-scanning confocal microscopy. (**A**) Schematic of the tri-scanning polarization microscope. (**B**) Comparison of FLIPs and translocation-based biosensors. Top row: Imaging of β2AR activation. Left: Images of a cell expressing a FLIP (NB80-eGFP-hRas), acquired before and after β2AR activation by isoproterenol. Middle: Fluorescence microscopy images of a cell expressing a translocation-based biosensor (NB80-eGFP), before and after β2AR activation. Kymographs show the time course of biosensor responses (LD or translocation, respectively) in the indicated cell regions. Right: Comparison of kinetics of responses by the two types of biosensors. Bottom row: Comparisons of kinetics of responses of FLIPs and translocation biosensors of activation of G protein Gai1 (based on the peptide KB1753), μOR (nanobody NB33), and β2AR (NB80Lite). Mean values and SDs are shown, $n = 10$ cells. (**C**) Imaging of activity of nonmodified, endogenously expressed G_i. Left: A cell overexpressing KB1753-eGFP-HRas and μOR-IRES-mCherry before and after application of a μOR agonist (DAMGO) and after application of an antagonist (naloxone). The kymographs show LD of the marked areas. Right: Kinetics of responses of KB1753-eGFP-hRas to activation and inactivation of endogenously expressed G_i (means ± 95% confidence intervals, $n = 12$ cells). Scale bars, 5 μm. ROI, region of interest.

goal of real-time imaging of the activity of nonmodified, endogenously expressed G proteins with subcellular resolution, making a substantial step toward imaging the activity of endogenously expressed G proteins in response to stimulation of endogenously expressed GPCRs, ideally by endogenous agonists.

The combination of FLIPs with tri-scanning confocal microscopy opens possibilities in imaging of cell signaling. The high speed and sensitivity of both the biosensors and the microscopy setup allows temporally accurate real-time imaging of fast biomolecular processes, even in nonmodified, endogenously expressed proteins, unachievable using traditional sensors and imaging methods.

DISCUSSION

We have developed a previously unexploited way of biosensing by taking advantage of the optical directionality of fluorescent molecules. Embodied in the FLIP design, our approach results in a large, widely applicable and exceedingly simple class of biosensors that can report on numerous scientifically and pharmacologically important molecular processes. The biosensors will provide previously inaccessible insights into many cell signaling events.

The FLIP design offers a powerful combination of desirable properties. The approach does not require any modification of the molecular targets, is sensitive enough to detect even the activity of endogenously expressed proteins, and shows subsecond response times. The kinetic properties of FLIPs are comparable to the fast biosensors of the GRAB design (*46*, *47*) that rely on insertion of a cpFP into a GPCR. While some highly optimized GRABs exhibit larger responses ($\Delta F/F$) (*48*, *49*) than FLIPs, FLIPs provide a ratiometric readout that allows not only observing dynamic changes but also assessing the basal state. The sensitivity of FLIPs, combined with their ability to report on function of nonmodified targets, has allowed imaging of activity of an endogenously expressed G protein. We have shown that a single FLIP can not only report on the presence or absence of a target, but, uniquely, it can also distinguish among several states of the target, yielding more information than other types of biosensors. This ability allowed us to unambiguously demonstrate a pronounced conformational change in GPCR-arrestin complexes and to show that it occurs specifically in endosomes. Our results reveal a previously undescribed event in the mechanisms of signaling by GPCRs, an exceedingly large and important class of proteins. The ability to perform such observations in living cells, in real time, in signaling proteins that have not been modified in any way, sets a standard in microscopy imaging of protein signaling.

These abilities are further enhanced by the combination of FLIPs with fast tri-scanning LD microscopy and its high speed and sensitivity. We have demonstrated the power of the approach by real-time imaging of FLIPs and corresponding translocation-based sensors, as well as by imaging the activity of an endogenously expressed Gαi, a breakthrough in functional G protein imaging, opening a hitherto unexploited avenue toward imaging G protein activity in physiological context. The results demonstrate superior response rates of FLIPs and an inability of translocation-based sensors to capture the dynamics of the observed molecular processes. Furthermore, translocation alone does not allow differentiating between several distinct forms of targets the way FLIPs can (e.g., distinguishing between different forms of GPCR-arrestin complexes; Fig. 5). However, some translocation-based sensors do exhibit LD upon their target binding and might yield structural information when observed by LD microscopy.

The FLIP biosensors do also have limitations. LD microscopy relies on the shape of the cell membrane, which can be irregular. However, as we show (Fig. 6), this does not prevent facile quantitation of LD responses. Furthermore, due to the mathematical relationship between LD and cell membrane orientation, accurate $\log_2(r_0)$ determinations can be made (*19*) even using very small suitable sections of a cell membrane, which do not need to be ideally oriented. LD of a membrane may be affected by the juxtaposition of another cell. Thus, to maintain consistency, as well as to avoid agonist/antagonist accessibility issues, we used membranes exposed to the medium for image analyses. LD microscopy does require the observed features to be of large enough size for their outline to be discernible. Another apparent FLIP limitation is the requirement for the target to be membrane associated. However, our previous work has already shown that changes in LD of membrane-tethered constructs can be triggered even by cytoplasmic events (*8*) such as changes in calcium ion concentration. Thus, FLIPs should respond by LD changes even to binding cytoplasmic targets, because these can also affect the orientation or mobility of the fluorescent moiety. Thus, FLIPs might prove to be useful also to studies of cytoplasmic signaling cascades, including various kinase and phosphatase activities. However, even with cytoplasmic targets, the biosensors will have to be tethered to a cellular structure. Last, by binding to their targets, FLIPs might sequester the targets from downstream signaling. Nonetheless, choosing a suitable combination of FLIP concentration and binding affinity should allow overcoming this drawback. Therefore, FLIPs, in combination with polarization microscopy, present a substantial, widely applicable improvement over existing approaches.

To observe FLIPs, various polarization microscopy modalities can be used. We prefer imaging FLIPs by LD microscopy, implemented on a laser-scanning confocal microscope (*19*). This implementation combines the advantages of optical sectioning, a wide range of detection channels, and relatively (in comparison with fluorescence polarization microscopy) low depolarization by the objective lens and by the excited FP molecules (*15*). Nonetheless, it is also possible to use FLIPs with fluorescence polarization microscopy (fig. S10). Combining FLIPs with various implementations of polarization microscopy [including wide-field (*50*), multipoint (*51*), holographic (*52*), or super-resolution (*53*)], as well as with a growing range of publicly available software tools for polarization microscopy image analysis (*19*, *54*–*57*), promises to allow functional imaging in a wide range of biological contexts (*58*), from single-molecule studies in individual organelles or cellular compartments (*59*) to observations in transgenic animals (*8*) or living tissues. The possibilities are illustrated by our implementation of LD microscopy on a tri-scanning confocal microscope. The microscope's imaging speed, sectioning ability, and sensitivity combined with the fast and robust responses of the FLIP biosensors promise to allow real-time imaging of signaling by nonmodified G proteins and other signaling proteins in living tissues or even whole organisms, as well as applications in pharmaceutical drug screening and diagnostics.

By being compatible with a wide variety of affinity binders, anchoring moieties, linkers, and fluorescent molecules (potentially including self-labeling proteins), the FLIP design allows rapid development of numerous molecular biosensors. Furthermore, by drawing attention to optical directionality of FPs, our results will likely inspire other biosensor designs that take advantage of this fundamental property of fluorescent molecules. We hope that, in combination with tri-scanning LD microscopy and other modern imaging approaches,

the FLIP molecular design will ultimately transform polarization-resolved fluorescence microscopy, a simple, long overlooked optical microscopy modality, into a mainstream tool of functional biomolecular imaging, under conditions close to natural.

Apart from illustrating the performance of FLIP biosensors, our results also highlight the ability of tri-scanning confocal microscopy to accommodate distinct imaging modalities and to elevate the capacity of fluorescent biosensors. In some ways, tri-scanning eschews traditional efforts at maximizing resolution and overall optical perfection. Instead, it simplifies the optical design (slightly reducing image resolution along the *z* axis) while providing flexibility, high sensitivity, low photobleaching, and speed that rivals or exceeds that of spinning disk microscopy. Furthermore, by being accommodating to a variety of imaging modalities and molecular photophysical phenomena, the tri-scan design delivers exceptional qualities for molecular biosensing. Thus, we believe that, by virtue of its overall simplicity, sensitivity, and versatility, the combination of FLIPs with tri-scanning microscopy is just an initial demonstration of a powerful, accessible microscopy biosensing platform that will in the future allow efficient exploitation of a wide range of photophysical detection principles (FRET, fluorescence lifetime, photoblinking, photoswitching, super-resolution, etc.) and biosensor designs, with marked impact not only on our basic understanding of cell biology but also on pharmaceutical drug development and testing.

MATERIALS AND METHODS

Experimental design

To observe molecular processes of cell signaling, we prepared plasmid constructs and transfected them into mammalian cells. We then observed the transfected cells by LD confocal microscopy, processed the acquired images to obtain quantitative data, and statistically evaluated the imaging data.

Constructs

The plasmids encoding KB1753-eGFP-HRas and GAP43-eGFP-KB1753 [both in the pcDNA3.1(+) backbone] were prepared by gene synthesis (GenScript). The constructs were designed to allow excision of the DNA encoding the affinity binding moiety, the FP moiety, and the membrane-targeting moiety by a unique combination of restriction endonucleases (Eco RI/Xho I, Xho I/Bam HI, and Bam HI/Not I, respectively). Other FLIPs were prepared from the two starting plasmids by a suitable restriction digestion, followed by ligation of the desired DNA fragment, obtained through gene synthesis (GenScript). In some cases, preliminary experiments were performed using constructs kindly provided by A. Shukla [plasmids containing NB32, βArr1, βArr1(FLD), and B2R] and M. von Zastrow (NB33). As FPs, we used eGFP bearing the dimerization-preventing mutations A206K, L221K, and F223R. Circularly permuted FPs (cpmTurq2 and cpsfGFP) were based on superfolder mTurquoise2 and sfGFP2. FLIP targets were cloned into a pcDNA3.1(+) plasmid backbone containing either internal ribosomal entry site (IRES)–mCherry or IRES-mTurquoise2, allowing identification of target-expressing cells by fluorescence of the bicistronically expressed FP, while the targets themselves bore no modifications. Constitutively active mutants [Gαi1(Q204L), Gαq(Q209L), Gαs(Q227L), and RacA(Q61L)] were prepared by polymerase chain reaction (PCR) mutagenesis. NB80Lite was created by introducing mutations H52S, S56G, T57S, and N58A into NB80-eGFP-HRas by PCR mutagenesis. Plasmids encoding translocation-based sensors were prepared from corresponding FLIPs, by removing the membrane anchor sequences by PCR. All FLIP protein sequences are provided in table S3.

Mammalian cell culture

HEK293 cells obtained from American Type Culture Collection, passaged less than 15 times, were used throughout. Cells were regularly tested for mycoplasma by Hoechst staining. For imaging, cells were plated in 8- or 18-well imaging slides (iBidi) and transfected with the desired plasmid (0.5 μg per well) using Lipofectamine 3000 (Thermo Fisher Scientific) and the manufacturer's procedure. Cells were observed by LD microscopy 1 or 2 days after transfection. During imaging, GPCR agonists (DAMGO, isoproterenol, and bradykinin; final concentrations, 10 μM) and antagonists (naloxone and propranolol; final concentrations, 100 μM) were added by manual pipetting. Agonists and antagonists were purchased from Sigma-Aldrich.

Microscopy

Initial LD imaging was carried out as described previously (*8*, *19*), on a customized laser-scanning confocal microscope (Olympus FV1200), equipped with a polarization modulator (RPM-2P, Innovative Bioimaging, L.L.C.) alternating the excitation light linear polarization between acquisition of subsequent pixels by the microscope. The objective (UApoN340, numerical aperture of 1.15, Olympus, Japan) and pixel dwell times of 10 μs were used throughout. Cells expressing constructs bearing mTurqoise2 were imaged using 405-nm illumination and a 450- to 550-nm emission window. Cells expressing constructs containing eGFP were imaged using 488-nm illumination, and emission at 510 to 610 nm was collected. Cells expressing constructs with mScarlet and mCherry were imaged using 543-nm excitation; emission at 560 to 650 nm was collected. Two-photon LD imaging was carried out as described previously (*19*), using wavelengths of 850 nm (mTurq2), 900 nm (eGFP), and 1000 nm (mScarlet). For structural analyses, cells were swelled by addition of hypotonic medium (Dulbecco's modified Eagle's medium diluted 10× in water) before imaging. The resulting images were processed and analyzed as described (*19*), using Fiji and publicly available macros for LD image analysis, as well as Polaris+ software (Innovative Bioimaging, L.L.C.). Briefly, each raw image (containing information on fluorescence intensity acquired with both excitation polarizations) was deconvolved into a pair of images, each holding information on fluorescence intensity acquired with one polarization of the excitation light. For LD visualization, the images acquired with horizontal and vertical polarization of the excitation light were colored magenta and green, respectively, and the color saturation was adjusted to match the desired range of LD. To quantitate LD, parts of images containing the cell membrane were semiautomatically segmented, and the shape of the cell outline was approximated by a spline. For each segmented pixel, the dichroic logratio [$\log_2(r) = \log_2(F_h/F_v)$] and membrane orientation (angle θ; slope at the nearest point on the spline approximating the cell outline) were determined as described previously. The observed $\log_2(F_h/F_v)$ versus θ data were used for determining (by fitting) the value of $\log_2(r_0)$, that is, the value of $\log_2(F_h/F_v)$ in a membrane whose normal is oriented horizontally within the image ($\theta = 0$). The published software tools and procedures (*19*) allowed accurate determinations of $\log_2(r_0)$ even in the absence of ideally oriented sections of the cell outline in an image. At least 10 cells were observed and analyzed for each construct or combination of constructs, over at least three different

weeks. Distributions of the $\log_2(r_0)$ values for a large majority of our experiments were normal (according to Anderson-Darling test and D'Agostino and Pearson test). To maintain consistency, we treated all $\log_2(r_0)$ values as normally distributed.

Fluorescence polarization imaging was carried out using a modified Olympus FV1200 confocal microscope. For illumination, the optical fiber with a collimator was detached from the microscope body, and a Glan-Taylor polarizer (GT10-A, Thorlabs) and an achromatic quarter-wave plate (WP140HE, Edmund Optics) oriented to ensure circularly polarized sample illumination were placed in the laser beam path before the beam was steered into the scanning unit. In the detector unit, a dichroic beam splitter assembly was replaced by a polarizing beam splitter cube (PBS201, Thorlabs) flanked by sheet polarizers (XP42, Edmund Optics; extinction ratio, 9000:1). The extent of fluorescence polarization was quantified analogously to that of LD, by observing the logratio of the two fluorescence intensities along the cell outline and determining, by fitting, the value of $\log_2(r_0)$, that is, $\log_2(F_{\parallel}/F_{\perp})$ at membrane sections oriented horizontally in the image ($\theta = 0$).

Fast LD imaging was performed using a simplified design of the TriScan line-scanning confocal microscope (*44*). The microscope used a single resonant scanner (SC20, by EOPC, operating at 212 Hz) to (i) scan a laser beam through the sample, (ii) descan the fluorescence before its passage through the confocal assembly, and (iii) scan the fluorescence across the camera sensor. For excitation, the laser beam (CellX, Coherent; 405, 488, and 561 nm; typically, 5 mW) was passed through a Glan-laser polarizer (GL15-A, Thorlabs) and a polarization modulator (1P-FL!Pper, Innovative Bioimaging). After 5× expansion and passage through a cylindrical lens (CL; focal length $f = 250$ mm), the beam was reflected by a polychroic mirror (zt440-488-561-635rpc, Chroma) and the scanning mirror. The beam was then relayed through a scan lens (L1, $f = 150$ mm) and a tube lens (L2, $f = 175$ mm), so that, after passing through the objective lens, it would form a line in the focal plane. Fluorescence (after passing through lenses L2 and L1) was descanned by the scanning mirror, separated from illumination by the polychroic mirror, and steered through a confocal assembly (a slit flanked by L3 and L3′, both $f = 125$ mm) back to the scanning mirror. A 30 μm–by–10 mm slit (S30LK, Thorlabs) was used in the confocal assembly. Last, the scanning mirror scanned the fluorescence through a camera lens (L4, $f = 400$ mm) onto the detector chip of a camera (iXon 888, Andor). All lenses (except for CL) were achromatic doublets with 350- to 700-nm antireflection coating (Thorlabs). The polarization modulator was triggered by the camera to alternate the polarization of the excitation light between acquisition of individual images, acquired at 150-ms exposition times. During scanning, laser power was continuously modulated within each scanning cycle to achieve homogeneous sample illumination despite periodic changes in scanning angular velocity. LD was visualized and quantitated using ImageJ and published polarization microscopy macros (*19*). At least 10 cells were observed and analyzed for each construct or combination of constructs, over at least three different weeks.

Statistical analysis

LD imaging data were statistically evaluated as in our previous studies (*8*, *19*). Namely, for each experiment, the extent of LD was characterized as dichroic logratio [$\log_2(r_0)$] in at least 10 cells, observed in 3 separate weeks. Distributions of the $\log_2(r_0)$ values for a large majority of our experiments were normal (according to Anderson-Darling test and D'Agostino and Pearson test). To maintain consistency, we treated all $\log_2(r_{max})$ values as normally distributed. Experimental results were characterized by mean values and standard errors of the mean. Statistical significance was assessed by paired or unpaired *t* tests, as appropriate.

Supplementary Materials

The PDF file includes:
Figs. S1 to S10
Tables S1 to S3
Legends for movies S1 to S5

Other Supplementary Material for this manuscript includes the following:
Movies S1 to S5

REFERENCES

1. V. S. Ovechkina, S. M. Zakian, S. P. Medvedev, K. R. Valetdinova, Genetically encoded fluorescent biosensors for biomedical applications. *Biomedicine* **9**, 1528 (2021).
2. A. Bondar, J. Lazar, Optical sensors of heterotrimeric G protein signaling. *FEBS J.* **288**, 2570–2584 (2021).
3. R. Irannejad, J. C. Tomshine, J. R. Tomshine, M. Chevalier, J. P. Mahoney, J. Steyaert, S. G. Rasmussen, R. K. Sunahara, H. El-Samad, B. Huang, M. von Zastrow, Conformational biosensors reveal GPCR signalling from endosomes. *Nature* **495**, 534–538 (2013).
4. C. Avet, A. Mancini, B. Breton, C. L. Gouill, A. S. Hauser, C. Normand, H. Kobayashi, F. Gross, M. Hogue, V. Lukasheva, S. St-Onge, M. Carrier, M. Héroux, S. Morissette, E. B. Fauman, J.-P. Fortin, S. Schann, X. Leroy, D. E. Gloriam, M. Bouvier, Effector membrane translocation biosensors reveal G protein and βarrestin coupling profiles of 100 therapeutically relevant GPCRs. *eLife* **11**, e74101 (2022).
5. S. Inoué, O. Shimomura, M. Goda, M. Shribak, P. Tran, Fluorescence polarization of green fluorescence protein. *Proc. Natl. Acad. Sci. U.S.A.* **99**, 4272–4277 (2002).
6. J. Myšková, O. Rybakova, J. Brynda, P. Khoroshyy, A. Bondar, J. Lazar, Directionality of light absorption and emission in representative fluorescent proteins. *Proc. Natl. Acad. Sci. U.S.A.* **117**, 32395–32401 (2020).
7. A. M. Vrabioiu, T. J. Mitchison, Structural insights into yeast septin organization from polarized fluorescence microscopy. *Nature* **443**, 466–469 (2006).
8. J. Lazar, A. Bondar, S. Timr, S. J. Firestein, Two-photon polarization microscopy reveals protein structure and function. *Nat. Methods* **8**, 684–690 (2011).
9. Z. Han, L. Jin, F. Chen, J. J. Loturco, L. B. Cohen, A. Bondar, J. Lazar, V. A. Pieribone, Mechanistic studies of the genetically encoded fluorescent protein voltage probe ArcLight. *PLOS ONE* **9**, e113873 (2014).
10. C. A. Valades Cruz, H. A. Shaban, A. Kress, N. Bertaux, S. Monneret, M. Mavrakis, J. Savatier, S. Brasselet, Quantitative nanoscale imaging of orientational order in biological filaments by polarized superresolution microscopy. *Proc. Natl. Acad. Sci. U.S.A.* **113**, E820–E828 (2016).
11. N. Nakai, K. Sato, T. Tani, M. Kawagishi, H. Ka, K. Saito, S. Terada, Development of nanobody-based POLArIS orientation probes enabled multi-color/multi-target orientation imaging in living cells. *Biochem. Biophys. Res. Commun.* **565**, 50–56 (2021).
12. M. McQuilken, M. S. Jentzsch, A. Verma, S. B. Mehta, R. Oldenbourg, A. S. Gladfelter, Analysis of septin reorganization at cytokinesis using polarized fluorescence microscopy. *Front. Cell Dev. Biol.* **5**, 42 (2017).
13. S. C. Warren, A. Margineanu, M. Katan, C. Dunsby, P. M. W. French, Homo-FRET based biosensors and their application to multiplexed imaging of signalling events in live cells. *Int. J. Mol. Sci.* **16**, 14695–14716 (2015).
14. A. Bondar, J. Lazar, Dissociated GαGTP and Gβγ protein subunits are the major activated form of heterotrimeric Gi/o proteins. *J. Biol. Chem.* **289**, 1271–1281 (2014).
15. A. Bondar, J. Lazar, The G protein Gi1 exhibits basal coupling but not preassembly with G protein-coupled receptors. *J. Biol. Chem.* **292**, 9690–9698 (2017).
16. M. Maziarz, J.-C. Park, A. Leyme, A. Marivin, A. Garcia-Lopez, P. P. Patel, M. Garcia-Marcos, Revealing the activity of trimeric G-proteins in live cells with a versatile biosensor design. *Cell* **182**, 770–785.e16 (2020).
17. C. A. Johnston, E. S. Lobanova, A. S. Shavkunov, J. Low, J. K. Ramer, R. Blaesius, Z. Fredericks, F. S. Willard, B. Kuhlman, V. Y. Arshavsky, D. P. Siderovski, Minimal determinants for binding activated Gα from the structure of a Gαi1–peptide dimer. *Biochemistry* **45**, 11390–11400 (2006).
18. J. T. Stickney, M. A. Booden, J. E. Buss, "Targeting proteins to membranes, using signal sequences for lipid modifications," in *Methods in Enzymology* (Elsevier, 2001), vol. 332, pp. 64–77.
19. A. Bondar, O. Rybakova, J. Melcr, J. Dohnálek, P. Khoroshyy, O. Ticháček, Š. Timr, P. Miclea, A. Sakhi, V. Marková, J. Lazar, Quantitative linear dichroism imaging of molecular

processes in living cells made simple by open software tools. *Commun. Biol.* **4**, 189 (2021).
20. S. Timr, J. Brabec, A. Bondar, T. Ryba, M. Zelezny, J. Lazar, P. Jungwirth, Nonlinear optical properties of fluorescent dyes allow for accurate determination of their molecular orientations in phospholipid membranes. *J. Phys. Chem. B* **119**, 9706–9716 (2015).
21. C. Ast, J. Foret, L. M. Oltrogge, R. De Michele, T. J. Kleist, C.-H. Ho, W. B. Frommer, Ratiometric Matryoshka biosensors from a nested cassette of green- and orange-emitting fluorescent proteins. *Nat. Commun.* **8**, 431 (2017).
22. J. Goedhart, D. Von Stetten, M. Noirclerc-Savoye, M. Lelimousin, L. Joosen, M. A. Hink, L. Van Weeren, T. W. Gadella Jr., A. Royant, Structure-guided evolution of cyan fluorescent proteins towards a quantum yield of 93%. *Nat. Commun.* **3**, 751 (2012).
23. B. Melkes, L. Hejnova, J. Novotny, Biased μ-opioid receptor agonists diversely regulate lateral mobility and functional coupling of the receptor to its cognate G proteins. *Naunyn Schmiedebergs Arch. Pharmacol.* **389**, 1289–1300 (2016).
24. M. Stoeber, D. Jullié, B. T. Lobingier, T. Laeremans, J. Steyaert, P. W. Schiller, A. Manglik, M. von Zastrow, A genetically encoded biosensor reveals location bias of opioid drug action. *Neuron* **98**, 963–976.e5 (2018).
25. S. G. Rasmussen, H.-J. Choi, J. J. Fung, E. Pardon, P. Casarosa, P. S. Chae, B. T. DeVree, D. M. Rosenbaum, F. S. Thian, T. S. Kobilka, A. Schnapp, I. Konetzki, R. K. Sunahara, S. H. Gellman, A. Pautsch, J. Steyaert, W. I. Weis, B. K. Kobilka, Structure of a nanobody-stabilized active state of the β2 adrenoceptor. *Nature* **469**, 175–180 (2011).
26. D. Wootten, A. Christopoulos, M. Marti-Solano, M. M. Babu, P. M. Sexton, Mechanisms of signalling and biased agonism in G protein-coupled receptors. *Nat. Rev. Mol. Cell Biol.* **19**, 638–653 (2018).
27. J. Van Gastel, J. O. Hendrickx, H. Leysen, P. Santos-Otte, L. M. Luttrell, B. Martin, S. Maudsley, β-Arrestin based receptor signaling paradigms: Potential therapeutic targets for complex age-related disorders. *Front. Pharmacol.* **9**, 1369 (2018).
28. N. G. Tsvetanova, R. Irannejad, M. von Zastrow, G protein-coupled receptor (GPCR) signaling via heterotrimeric G proteins from endosomes. *J. Biol. Chem.* **290**, 6689–6696 (2015).
29. T. J. Cahill III, A. R. Thomsen, J. T. Tarrasch, B. Plouffe, A. H. Nguyen, F. Yang, L.-Y. Huang, A. W. Kahsai, D. L. Bassoni, B. J. Gavino, J. E. Lamerdin, S. Triest, A. K. Shukla, B. Berger, J. Little IV, A. Antar, A. Blanc, C. X. Qu, X. Chen, K. Kawakami, A. Inoue, J. Aoki, J. Steyaert, J. P. Sun, M. Bouvier, G. Skiniotis, R. J. Lefkowitz, Distinct conformations of GPCR–β-arrestin complexes mediate desensitization, signaling, and endocytosis. *Proc. Natl. Acad. Sci. U.S.A.* **114**, 2562–2567 (2017).
30. N. R. Latorraca, J. K. Wang, B. Bauer, R. J. Townshend, S. A. Hollingsworth, J. E. Olivieri, H. E. Xu, M. E. Sommer, R. O. Dror, Molecular mechanism of GPCR-mediated arrestin activation. *Nature* **557**, 452–456 (2018).
31. A. H. Nguyen, A. R. Thomsen, T. J. Cahill III, R. Huang, L.-Y. Huang, T. Marcink, O. B. Clarke, S. Heissel, A. Masoudi, D. Ben-Hail, F. Samaan, V. P. Dandey, Y. Z. Tan, C. Hong, J. P. Mahoney, S. Triest, J. Little IV, X. Chen, R. Sunahara, J. Steyaert, H. Molina, Z. Yu, A. des Georges, R. J. Lefkowitz, Structure of an endosomal signaling GPCR–G protein–β-arrestin megacomplex. *Nat. Struct. Mol. Biol.* **26**, 1123–1131 (2019).
32. P. Sarma, V. N. Marková, N. Zaidi, A. Dalal, S. Mishra, M. K. Yadav, G. Mahajan, N. Roy, P. Miclea, J. Lazar, A. K. Shukla, A genetically-encoded nanobody sensor reveals conformational diversity in β-arrestins orchestrated by distinct seven transmembrane receptors. *Proc. Natl. Acad. Sci. U.S.A.* **122**, e2507384122 (2025).
33. B. Zimmerman, M. Simaan, M.-Y. Akoume, N. Houri, S. Chevallier, P. Séguéla, S. A. Laporte, Role of ssarrestins in bradykinin B2 receptor-mediated signalling. *Cell. Signal.* **23**, 648–659 (2011).
34. M. Simaan, S. Bédard-Goulet, D. Fessart, J.-P. Gratton, S. A. Laporte, Dissociation of β-arrestin from internalized bradykinin B2 receptor is necessary for receptor recycling and resensitization. *Cell. Signal.* **17**, 1074–1083 (2005).
35. M. E. Lamb, W. F. De Weerd, L. M. Leeb-Lundberg, Agonist-promoted trafficking of human bradykinin receptors: Arrestin-and dynamin-independent sequestration of the B2 receptor and bradykinin in HEK293 cells. *Biochem. J.* **355**, 741–750 (2001).
36. M. Haasemann, J. Cartaud, W. Müller-Esterl, I. Dunia, Agonist-induced redistribution of bradykinin B 2 receptor in caveolae. *J. Cell Sci.* **111**, 917–928 (1998).
37. A. Blaukat, A. Pizard, A. Breit, C. Wernstedt, F. Alhenc-Gelas, W. Muller-Esterl, I. Dikic, Determination of bradykinin B2 receptor in vivo phosphorylation sites and their role in receptor function. *J. Biol. Chem.* **276**, 40431–40440 (2001).
38. A. Pizard, A. Blaukat, W. Muller-Esterl, F. Alhenc-Gelas, R. M. Rajerison, Bradykinin-induced internalization of the human B2 receptor requires phosphorylation of three serine and two threonine residues at its carboxyl tail. *J. Biol. Chem.* **274**, 12738–12747 (1999).
39. J. Janetzko, R. Kise, B. Barsi-Rhyne, D. H. Siepe, F. M. Heydenreich, K. Kawakami, M. Masureel, S. Maeda, K. C. Garcia, M. von Zastrow, A. Inoue, B. K. Kobilka, Membrane phosphoinositides regulate GPCR-β-arrestin complex assembly and dynamics. *Cell* **185**, 4560–4573.e19 (2022).
40. S. D. Fried, J. W. Lewis, I. Szundi, K. Martinez-Mayorga, M. Mahalingam, R. Vogel, D. S. Kliger, M. F. Brown, Membrane curvature revisited—The archetype of rhodopsin studied by time-resolved electronic spectroscopy. *Biophys. J.* **120**, 440–452 (2021).
41. B. Hollins, S. Kuravi, G. J. Digby, N. A. Lambert, The c-terminus of GRK3 indicates rapid dissociation of G protein heterotrimers. *Cell. Signal.* **21**, 1015–1021 (2009).
42. K. C. Park, F. Rivero, R. Meili, S. Lee, F. Apone, R. A. Firtel, Rac regulation of chemotaxis and morphogenesis in Dictyostelium. *EMBO J.* **23**, 4177–4189 (2004).
43. J. Y. Chan, B. J. Hackel, D. Yee, Targeting insulin receptor in breast cancer using small engineered protein scaffolds. *Mol. Cancer Ther.* **16**, 1324–1334 (2017).
44. R. Van den Eynde, J. Verheyen, P. Miclea, J. Lazar, W. Vandenberg, P. Dedecker, The TriScan: Fast and sensitive 3D confocal fluorescence imaging using a simple optical design. bioRxiv 101113439 [Preprint] (2024). https://doi.org/10.3030/101113439.
45. S. Hardt, Rates of diffusion controlled reactions in one, two and three dimensions. *Biophys. Chem.* **10**, 239–243 (1979).
46. F. Sun, J. Zeng, M. Jing, J. Zhou, J. Feng, S. F. Owen, Y. Luo, F. Li, H. Wang, T. Yamaguchi, Z. Yong, Y. Gao, W. Peng, L. Wang, S. Zhang, J. du, D. Lin, M. Xu, A. C. Kreitzer, G. Cui, Y. Li, A genetically encoded fluorescent sensor enables rapid and specific detection of dopamine in flies, fish, and mice. *Cell* **174**, 481–496.e19 (2018).
47. M. Jing, P. Zhang, G. Wang, J. Feng, L. Mesik, J. Zeng, H. Jiang, S. Wang, J. C. Looby, N. A. Guagliardo, L. W. Langma, J. Lu, Y. Zuo, D. A. Talmage, L. W. Role, P. Q. Barrett, L. I. Zhang, M. Luo, Y. Song, J. J. Zhu, Y. Li, A genetically encoded fluorescent acetylcholine indicator for in vitro and in vivo studies. *Nat. Biotechnol.* **36**, 726–737 (2018).
48. T. Patriarchi, J. R. Cho, K. Merten, M. W. Howe, A. Marley, W.-H. Xiong, R. W. Folk, G. J. Broussard, R. Liang, M. J. Jang, H. Zhong, D. Dombeck, M. von Zastrow, A. Nimmerjahn, V. Gradinaru, J. T. Williams, L. Tian, Ultrafast neuronal imaging of dopamine dynamics with designed genetically encoded sensors. *Science* **360**, eaat4422 (2018).
49. Y. Zhuo, B. Luo, X. Yi, H. Dong, X. Miao, J. Wan, J. T. Williams, M. G. Campbell, R. Cai, T. Qian, F. Li, S. J. Weber, L. Wang, B. Li, Y. Wei, G. Li, H. Wang, Y. Zheng, Y. Zhao, M. E. Wolf, Y. Zhu, M. Watabe-Uchida, Y. Li, Improved green and red GRAB sensors for monitoring dopaminergic activity in vivo. *Nat. Methods* **21**, 680–691 (2024).
50. M. Kampmann, C. E. Atkinson, A. L. Mattheyses, S. M. Simon, Mapping the orientation of nuclear pore proteins in living cells with polarized fluorescence microscopy. *Nat. Struct. Mol. Biol.* **18**, 643–649 (2011).
51. S. Abrahamsson, M. McQuilken, S. B. Mehta, A. Verma, J. Larsch, R. Ilic, R. Heintzmann, C. I. Bargmann, A. S. Gladfelter, R. Oldenbourg, MultiFocus Polarization Microscope (MF-PolScope) for 3D polarization imaging of up to 25 focal planes simultaneously. *Opt. Express* **23**, 7734–7754 (2015).
52. T. Liu, K. de Haan, B. Bai, Y. Rivenson, Y. Luo, H. Wang, D. Karalli, H. Fu, Y. Zhang, J. FitzGerald, A. Ozcan, Deep learning-based holographic polarization microscopy. *ACS Photonics* **7**, 3023–3034 (2020).
53. L. Chen, X. Chen, X. Yang, C. He, M. Wang, P. Xi, J. Gao, Advances of super-resolution fluorescence polarization microscopy and its applications in life sciences. *Comput. Struct. Biotechnol. J.* **18**, 2209–2216 (2020).
54. W. F. Dean, T. J. Nawara, R. M. Albert, A. Mattheyses, OOPS: Object-oriented polarization software for analysis of fluorescence polarization microscopy images. *PLOS Comput. Biol.* **20**, e1011723 (2024).
55. E. Bruggeman, O. Zhang, L.-M. Needham, M. Körbel, S. Daly, M. Cheetham, R. Peters, T. Wu, A. S. Klymchenko, S. J. Davis, E. K. Paluch, D. Klenerman, M. D. Lew, K. O'Holleran, S. F. Lee, POLCAM: Instant molecular orientation microscopy for the life sciences. *Nat. Methods* **21**, 1873–1883 (2024).
56. A. Keikhosravi, Y. Liu, C. Drifka, K. M. Woo, A. Verma, R. Oldenbourg, K. W. Eliceiri, Quantification of collagen organization in histopathology samples using liquid crystal based polarization microscopy. *Biomed. Opt. Express* **8**, 4243–4256 (2017).
57. K. Zhanghao, X. Chen, W. Liu, M. Li, Y. Liu, Y. Wang, S. Luo, X. Wang, C. Shan, H. Xie, J. Gao, X. Chen, D. Jin, X. Li, Y. Zhang, Q. Dai, P. Xi, Super-resolution imaging of fluorescent dipoles via polarized structured illumination microscopy. *Nat. Commun.* **10**, 4694 (2019).
58. S. Brasselet, M. A. Alonso, Polarization microscopy: From ensemble structural imaging to single-molecule 3D orientation and localization microscopy. *Optica* **10**, 1486–1510 (2023).
59. M. P. Benoit, H. Sosa, "Use of single molecule fluorescence polarization microscopy to study protein conformation and dynamics of kinesin–microtubule complexes," in *Single Molecule Analysis: Methods and Protocols* (Springer, 2018), pp. 199–216.

Acknowledgments: We appreciate the help of Z. Vaitova with preparing constructs and performing microscopy imaging and the help of P. Khoroshyy with microscopy equipment. We thank A. Shukla (IIT Kanpur) and members of laboratory for providing constructs and for insightful discussions. We thank M. Garcia-Marcos (U. Boston) for providing constructs for preliminary experiments and for helpful discussions. We appreciate that M. von Zastrow (UCSF) provided constructs that served in FLIP development. We thank M. Sommer (ISAR Bioscience) for reading the manuscript and providing helpful suggestions. **Funding:** This work was supported by Ministry of Education, Youth and Science of the Czech Republic, grant LTAIN19167 (J.L.); Czech Science Foundation, grant 23-05983S (J.M.); European Innovation Council PathFinder project 101131014 UniSens (J.L.); Research Foundation-Flanders, grant G010723N (P.D.); Research Foundation-Flanders, grant 12A7225N (R.V.d.E.); and European Research Council, grant 101113439 (P.D.). Data

storage was provided by the CESNET LM2015042 facility under the program "Large Research, Development, and Innovation Infrastructures." **Author contributions:** P.M. designed and prepared constructs; carried out microscopy imaging, data processing, and analyses; and contributed to writing the paper. V.N.-M. performed imaging, data processing, and analyses. R.V.d.E. and W.V. contributed to the design and construction of the tri-scanning LD microscope. A.S. developed and investigated FLIPs of IR activity. A.B. inspired the idea of FLIPs and supervised experiments. J.M. performed quantitative analyses and interpretation of LD measurements. P.D. contributed expertise on tri-scanning microscopy and edited the manuscript. J.L. formulated, directed, and managed the project; provided technical expertise; designed constructs; designed and constructed the simplified tri-scanning polarization microscope; and wrote the manuscript, with input from the other coauthors. **Competing interests:** J.L. is the founder and owner of Innovative Bioimaging, s.r.o., and Innovative Bioimaging, L.L.C., companies commercializing tools for LD microscopy. P.M. and V.N.-M. are employees of Innovative Bioimaging, s.r.o. The FLIP biosensors are subject of an EPO patent application (EP212109717.4, J.L.). The constructs described in this manuscript are available for noncommercial uses upon request. The terms "fluorescence anisotropy and linear dichroism probes," "FLIP," and "FLIPs" were contributed by Innovative Bioimaging, s.r.o., which may claim copyright. The TriScan microscope design is subject to an EPO patent (EP4437377A1, KU Leuven) and patent applications (USPTO 2025020899A1, KU Leuven; PCT/CZ2024/050038, Innovative Bioimaging, s.r.o.). The authors declare that they have no other competing interests. **Data and materials availability:** All raw imaging data have been deposited to Zenodo (https://doi.org/10.5281/zenodo.17052982). ImageJ macros used for image processing and quantitative analysis are publicly available (https://doi.org/10.5281/zenodo.4383287). All constructs are available for a nominal fee from Innovative Bioimaging, s.r.o. (www.innovativebioimaging.com). The constructs can be provided by P.M.'s pending scientific review and a completed material transfer agreement through Innovative Bioimaging, s.r.o. Requests for the constructs should be submitted to flips@innovativebioimaging.com.

Submitted 13 June 2025
Accepted 15 December 2025
Published 16 January 2026
10.1126/sciadv.adz5662

ScienceAdvances

FLIPs: Genetically encoded molecular biosensors for functional imaging of cell signaling by linear dichroism microscopy

Paul Miclea, Vendula Nagy-Marková, Robin Van den Eynde, Wim Vandenberg, Alina Sakhi, Alexey Bondar, Jitka Myšková, Peter Dedecker, and Josef Lazar

Sci. Adv. **12** (3), eadz5662. DOI: 10.1126/sciadv.adz5662